Microwave spectrometry for the evaluation of in-stent restenosis

Author: Martí Checa Nualart
Grup de Magnetisme, Departament de Física Fonamental, Facultat de Física, Universitat de Barcelona, Martí i Franquès 1, planta 4, edifici nou, ES-08028 Barcelona (Spain).

Our purpose is to assess the feasibility of microwave spectrometry in the detection of in-stent restenosis, based in noting a resonant frequency shift for coronary stents. The aim of this work is to get closer towards a possible medical applicability for implanted stents. Microwave absorbance spectra between 0.2 and 1.8 GHz were acquired for the different stages of ISR model we fabricate. All the spectra were obtained in a water-based phantom simulating human chest. Rotating each sample over 360º, 2D absorbance diagrams were generated as a function of the frequency and the rotation angle. Finally with a few adjustments the same system provides similar 2D absorbance diagrams of stents immersed in different fluids such as sunflower oil, and filled in with different materials. We show that no frequency shift is observed in a stent with ISR. Even though the shift is found when changing the external medium of the stent, it seems that some kind of shielding of the electromagnetic fields inside the stents take place at the wavelengths we use, making impossible to detect diseases happening inside the stent. Motivated by the discouraging results of the ISR test we designed a series of more specific experiments in order to evaluating the effect in the resonant frequencies of the variation in dielectric permittivity of the material we place inside the stent. Thus, finding no differences when changing the medium inside the stent, we conclude that there is a shielding of the radiation inside the device. Thinking of other non ionizing methods to detect ISR will be necessary. Computational software using FDTD methods might be helpful.

I. INTRODUCTION:

Frequently, patients with atherosclerotic blood vessels are implanted with medical prosthetic devices known as "stents" [1]. The most common complication arising from stent implantation is called in-stent restenosis (ISR) [2] and can be understood like if the vessel, recognizing the stent as a others, starts growing up while wrapping the stent internally and making the blood flow across the vessel increasingly difficult [see Fig 1].

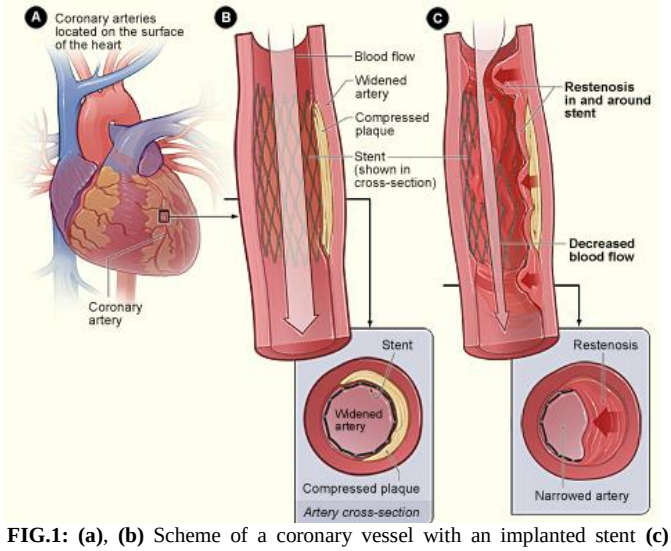

FIG.1: (a), **(b)** Scheme of a coronary vessel with an implanted stent **(c)** Subsequent ISR developing (taken from [3]).

Nowadays, doctors use ionizing techniques like x-ray angiography or invasive methods like intravascular ultrasound to detect ISR even though it is harder to detect it as more time has passed since the stent implantation.

Recently it has been proved by means of microwave spectrometry (MWS) that such devices exhibit characteristic resonant frequencies in their microwave absorbance spectra which reflect changes in the stent structure [4]. MWS is based in modeling the stent as a dipole antenna of length ($L = a\ell$) being able to predict its resonant frequencies as follows:

$$f_n = \frac{nc}{2a\ell\sqrt{\varepsilon_r\mu_r}} \qquad (1)$$

Where ε_r and μ_r are respectively the relative permittivity and permeability of the dipole antenna surrounding medium, c is the speed of light in vacuum, ℓ is the length of the stent, a is a scaling factor and n is the resonance mode. The change in the stent surrounding tissue between healthy and ISR situations, should be observed in a shift for the f_n, due to the variation of ε_r between healthy and ISR characteristic tissues. In contrast with the current detecting techniques MWS produces no harm to the patient.

II. THEORETICAL PREDICTIONS:

First of all, we want to calculate the expected shift that characteristic f_n will suffer when developing ISR. We are going to find an upper-bound for it, considering the relative change of the medium when the stent is wrapped in blood (healthy situation) or in blood vessel tissue (ISR situation). Knowing the different electric permittivity as a function of frequency for both tissues [5], we can calculate the new placement of resonant frequency and its shift, using Eq. (1):

$$f'_n = f_n\sqrt{\frac{\varepsilon_r\mu_r}{\varepsilon'_r\mu'_r}} \qquad (2)$$

Where f'_n is the resonant frequency in the medium with ε'_r and μ'_r, and f_n is the resonant frequency in the medium with ε_r and μ_r. Given that blood and blood vessels are non-magnetic ($\mu_r = \mu'_r = 1$), we are going to focus on the difference in permittivity which in our frequencies range takes shape of Fig.2(a), allowing us to calculate $f'_1{}^{\text{vessel}}$ and $f_1{}^{\text{blood}}$. Using Eq. (2) we have also calculated the shift ($\Delta = f'_1{}^{\text{vessel}} - f_1{}^{\text{blood}}$) between f'_1 and f_1 as a function of the frequency for the same stent measured in air ($\varepsilon_r = 1$) obtaining Fig. 2(b).

The Δ values found are in the order of magnitude of the tenths of GHz, which means that we need a setup precision of hundredths of GHz, to be capable of differentiating the two states. With the setup used in the present work the frequency precision is in the order of hundredths of GHz even MHz. So in principle we would be able to see the difference between healthy and ISR situations.

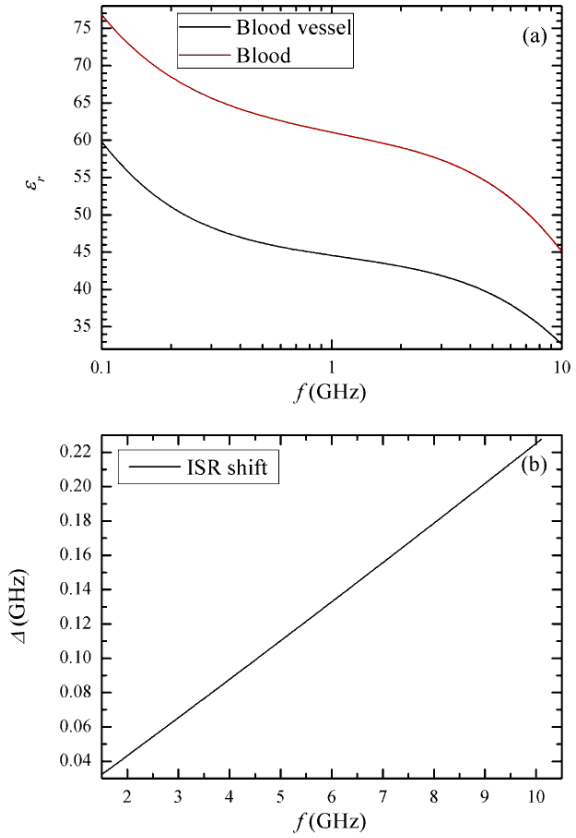

FIG. 2: (a) Electric permittivity of blood and blood vessel tissues as a function of frequency (axis in logarithmic scale). **(b)** Shift as a function of the stent resonant frequency in open air conditions.

We can draw that short stents should feature a bigger Δ than longer stents, due to the fact that short stents have higher resonant frequencies, than the longer ones [see Eq. 1]. But for the moment we can identify resonant frequencies better (sharper and higher) in long stents than in short stents, so we will have to keep equilibrium between these two facts.

III. EXPERIMENTAL METHODS

The experimental part of the job it is divided in two separate stages. In the first part, called Restenosis Test (RT) we made an *ex-vivo* model for ISR, and tried to sight a change in the resonant frequency between a non pathological and ISR situation. In the second part, we designed a series of experiments in order to show a possible shielding of electromagnetic field inside the stents: Shielding Test (ST).

For both tests, we are going to use the same experimental setup [see Fig. 3]. To carry out the characterizations of the absorbance spectra, a pair of microwave antennas with a 2-18 GHz spectral range [6] was connected to a two-port vector network analyzer [7] via coaxial feed lines. Measurements were performed in a symmetrical configuration in which the center of the stent was placed at the midpoint of the line joining the antennas (optical axis), that were set in the opposite walls of a methacrylate box (20 x 10 x 9 cm^3) filled with different fluids depending in the test we are. To avoid reflection of the radiation sent to the stent, the antennas were embedded in the fluid filling the phantom through side holes. The samples were placed using a rotating sample holder controlled by a circuit board [8]. The stents were threaded through using a 0.30-mm-thick nylon filament, and were suspended from above. This setup provides the transmission coefficient between the two ports of the analyzer as a function of frequency $S_{12}(f)$, from which absorbance spectrum can be calculated as:

$$A(f) = 10 \log \frac{S_{\text{ref}}(f)}{S_{12}(f)}$$

Here, $S_{\text{ref}}(f)$ denotes the reference transmission coefficient acquired as a function of frequency with a stent perpendicular to the optical axis. Both $S_{12}(f)$ and $S_{\text{ref}}(f)$ are the average of 100 measurements of each magnitude. For every sample subsequent spectra were obtained in steps of 1.8º over 360º. As a result, coordinating the network analyzer (controlled by a homemade program [9]) with the motorized sample holder, absorbance spectrum diagrams $A(f,\varphi)$ were generated using graphing and data analysis software [10].

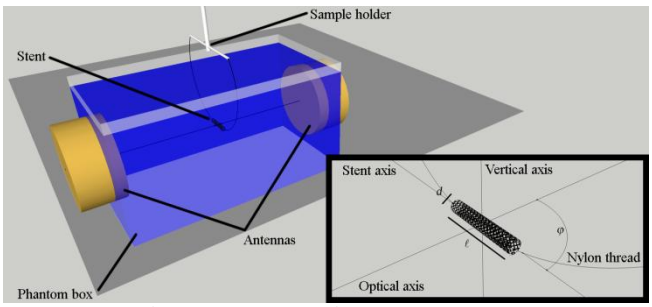

FIG. 3: Sketch of experimental setup for the microwave characterization of stents in tissue-like environment.

A bit of practice is needed to read the $A(f,\varphi)$ spectra and to identify the resonant frequencies properly. In air spectra, the stent resonant frequencies are very sharp and higher resonant modes are also observed. In contrast when we change to other mediums such as water, sometimes it is hard to recognize the resonances due to different facts: the resonance becomes wider and smaller making it harder to differentiate them from experimental noise. Furthermore, the resonant modes of the phantom itself can be confused with the stent resonant modes. Specifically in all the water absorbance graphics a 0.2 GHz width artifact appears around 1.4 GHz. We associate it to the resonant modes of the phantom. Data analyzer software [10] is used to generate the graphics and identify the resonant frequencies.

IV. RESTENOSIS TEST (RT)

IV- A. Modeling restenosis:

We design a model for ISR simulating healthy and a restenotic situations by combining stents with segments of swine carotid arteries. Working with swine vessels is a reasonable choice due to their similarity with the human ones. All measurements of RT have taken place with the phantom full of distilled water. The elements we are going to work with are:

Internal vessel	External vessel	Stent
I	E	S

FIG. 4: Cross-section sketches for the 3 elements of RT.

By introducing a stent within an external vessel segment we obtain a first "construct" able to reproduce a non restenotic setting (S+E). Threading now an internal vessel segment through the first construct, a second "construct" is obtained, representing typical restenotic scenery (I+S+E). We characterized these constructs and some complementary elements [see Fig. 5] by acquiring their *A(f,φ)* diagrams in the following order:

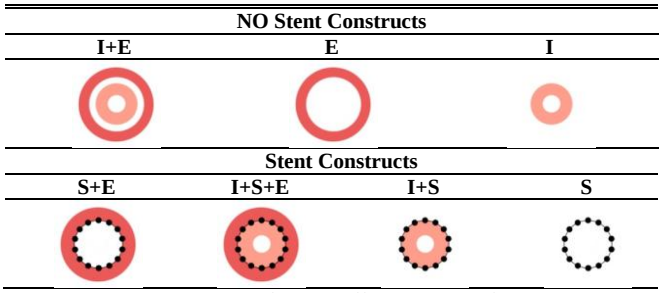

FIG. 5: Cross-section sketches for the different stages of the ISR *ex-vivo* model devised.

Where we have named the elements inside out, and the "plus" symbol indicates, that the internal element is entirely into the external element. Choosing these seven steps, we think it is a good way to see the possible contribution of each element to the absorbance graphics. We made the test with 5 different stents [see Tab. 1], obtaining similar results in each case, but presenting the results only for the Medtronic Integrity model [see Fig. 6]:

Model	Code	*d* (mm)	*ℓ* (mm)
Boston Scientific TAXUS Liberté	BTL	2.50	16.00
Boston Scientific TAXUS Liberté	BTL	3.50	28.00
Medtronic Resolute Integrity	MRI	2.95	8.00
Medtronic Resolute Integrity	MRI	3.05	12.00
Medtronic Integrity	MI	4.30	15.00

TAB. 1: Characteristics of the five stents investigated in the present work.

IV-B. Results and discussion of RT:

As it was expected, we found that "NO Stent Constructs" [see Fig. 5], are transparent to MWS watching no resonances in their *A(f,φ)* diagrams, due to the no conducting properties they own.

In contrast, for the "Stent Constructs" [see Fig. 5] a shift should be seen between the *A(f,φ)* spectra of S+E and I+S+E constructs, representing healthy and ISR situations, respectively. The magnitude of such shift should be around the tenth of GHz (Δ_{theor} = 0.1 GHz) since the first resonant mode of the measured stent in air appears at 5 GHz.

In Fig. 6 we present the spectrum of those 2 stages. The first resonant mode frequency for the healthy situation is: f_1 = (0.653 ± 0.002) GHz [see Fig. 6(a)] and the corresponding one in an ISR situation it is found at f'_1 = (0.658 ± 0.002) GHz [see Fig. 6(b)], what means a Δ_{exp} of (0.005 ± 0.004) GHz, which cannot be clearly referred to the different material inside the stent, but to little perturbations during the measurement process. This result shows the impossibility of detecting the illness with this technique.

Thus, we decided to go one step back and design a serial of experiments trying to see if the variation of the dielectric permittivity of the material inside the stents is affecting the resonant frequencies or not: Shielding Test (ST). We think that some kind of electromagnetic shielding might be taking place forbidding us to detect internal stent changes.

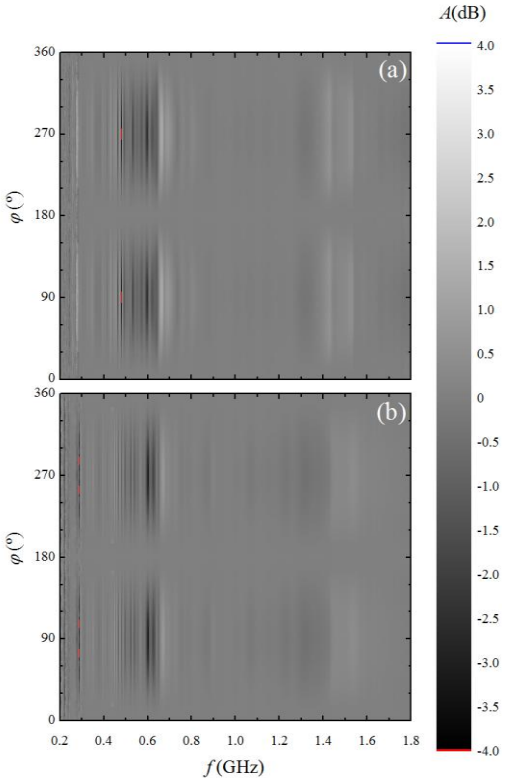

FIG. 6: (a) *A(f,φ)* spectrum for a healthy situation : (f_1= (0.653 ± 0.002) GHz) **(b)** *A(f,φ)* spectrum for a ISR situation (f'_1= (0.658 ± 0.002) GHz).

V. SHIELDING TEST (ST)

Depending on the medium the phantom is filled with (air, water or sunflower oil) we separate the shielding test in 3 stages. In each stage, we are going to get the *A(f,φ)* graphics of the stents , but fully stuffed with different fluids (olive oil or water), or a plastic material like parafilm. With this procedure we make the electric permittivity inside the stent change, expecting a frequency shift. The test has been performed with 2 stents only presenting the results for one of them (BTL, *d* = 3.5 mm, *ℓ* = 28 mm). Same results have been obtained with the other one (BTL, *d* = 2.5 mm, *ℓ* = 16 mm).

The methodology we followed to carry out the experiment was submerging the whole stent (already threaded through the nylon filament in the sample holder) in the selected fluid we want to have inside the device. Then, we took out the stent, leaving the liquid inside the core of it sustained due to surface tension. At this point, only sinking the sample in the phantom full of the other liquid we will have the construct ready for the measurement. Apart from introducing fluids or plastic inside the stent, we also made the test of introducing one stent inside another, to see the resonance of the smaller stent appears or remains shielded.

The values for the electric permittivity of the used materials are shown in Tab. 2, for each case they allow us to calculate the theoretical shift, using Eq. 2.

	Air	Olive oil	Sunflower oil	Parafilm	Distilled water
ε_r	1	3.1	3.1	2.2	78

TAB. 2: Electric permittivity for the materials used in ST.

V- A. Shielding in air:

Firstly, the phantom is going to be empty, and the stent's core full of: air, olive oil, parafilm, or another stent:

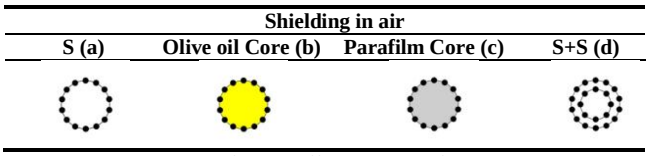

FIG. 7: Cross-section sketch for the different stages of shielding in air test.

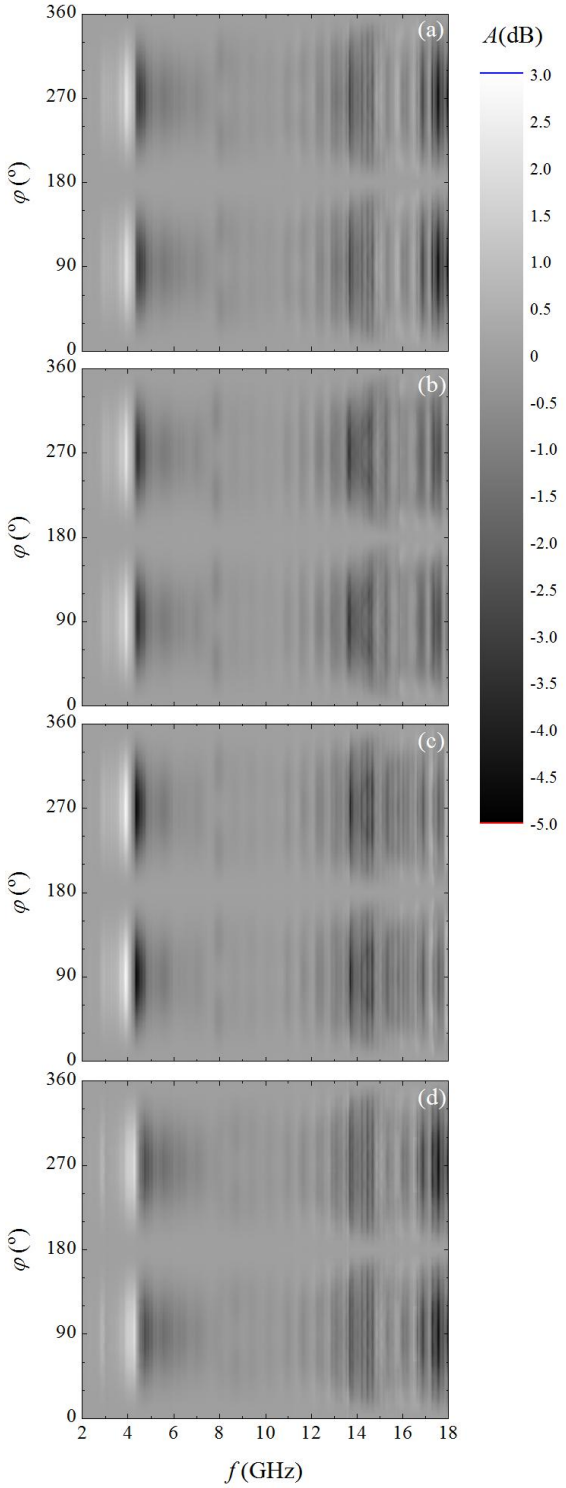

FIG. 8: *A(f,φ)* spectrums for shielding in air test **(a)** Stent in air **(b)** Stent in air with olive oil core **(c)** Stent in air with parafilm core **(d)** Stent in air inside another stent.

V- B. Shielding in fluids:

In that second part, the phantom is going to be filled with distilled water and the stent's core full of: water or olive oil (shielding in water).

Finally we filled the phantom with sunflower oil and the stent's core stuffed with sunflower oil or water respectively:

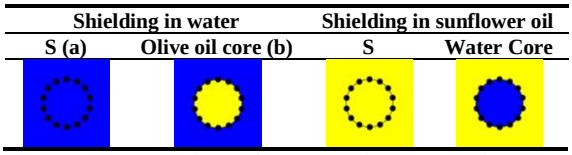

FIG. 9: Cross-section sketch for the four stages of shielding in fluid tests.

We only present the results for the shielding in water test; similar results are obtained for sunflower oil test:

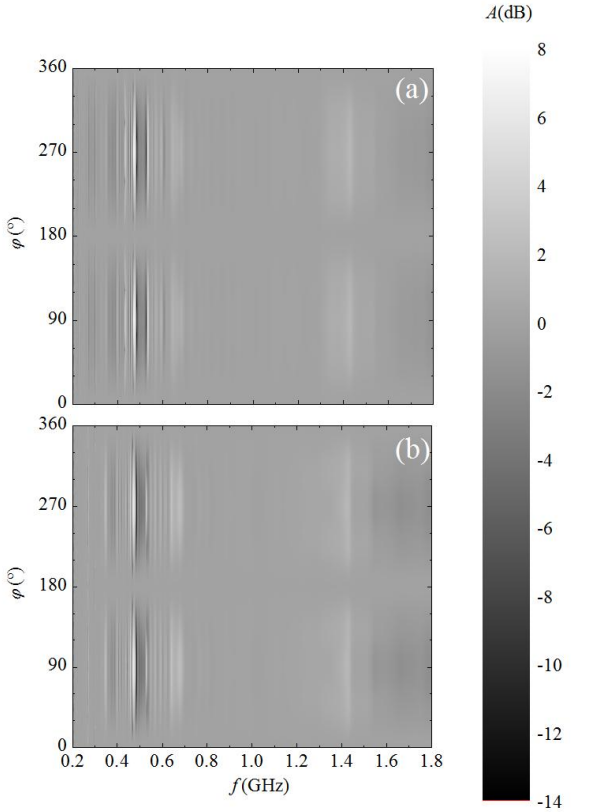

FIG. 10: *A(f,φ)* spectra for shielding in water **(a)** Stent in water **(b)** Stent in water with olive oil Core.

V- C. Results and discussion of ST:

In Figs. 8(a), 8(b) and 8(c), we see that the resonant frequencies for the absorbance graphics of the shielding in air are placed at 4.310 ± 0.002 GHz, suffering no shift when changing the medium in the core of the stent. Around 8 GHz, we clearly distinguish the second order resonant modes, not seen in the fluid spectrums.

Diagram in Fig. 8(d) only shows the resonant frequency of the external stent. The resonance of the internal stent remains shielded (should be situated at a frequency of 6.015 ± 0.002 GHz). A small shift observed in Fig. 8(d) can be caused by a possible physical contact between the two stents during the measurements. This contact could cause little changes in the course of the Eddy currents through the stent that are the responsible of the resonance.

When characterizing the stent underwater [see Fig. 10(a)], the resonant frequency measured in air, shifts down to 0.483 ± 0.002 GHz, and moves to 2.415 ± 0.002 GHz when is measured in sunflower oil. In both cases, no shift is observed when changing the material placed in the core of the device [see Fig. 10(b].

We think that the vertical lines appearing between 13 and 18 GHz in air diagrams, and 1.4 GHz in water spectrums are produced for the resonant modes of the own phantom itself, because they are always present in all the absorbance spectrums, even when measuring nothing, and they also appear around 9 GHz in sunflower oil graphics.

Thus, Shielding Test concludes that the shift seen when changing the medium we place the stent in it is only due to the stent's surrounding medium, not the medium in the core of the device. This behavior, allows us to understand the unexpected results found in Restenosis Test.

VI. CONCLUSIONS

Of this paper we can draw that even though when changing the surrounding medium of the stent, a shift in the resonant frequencies is observed according with theoretical predictions, MWS does not allow us to detect ISR, which was the main purpose of the work, due to electromagnetic shielding processes that take place inside the stent. Similar results are found when trying to see the inside of the stents with other electromagnetic techniques such as nuclear magnetic resonance [11, 12].

This shielding can be caused by many factors: the fact that the size of the stent conductive mesh (tenths of mm) is smaller than the wavelength of microwave radiation (cm), preventing the electromagnetic fields to reach the inner region of the artery. As well the high electromagnetic loss tangent of the mediums we fill the phantom with, makes the signal less powerful. Another possible reason is that the dipole antenna model we have been using, only takes into account the medium surrounding the antenna, not the medium of the antenna's structure. Computer simulating software using finite-difference time-domain (FDTD) methods might be interesting to understand the shielding better.

The improvement of the experimental setup in order to distinguish the resonant frequencies better could be helpful, especially when the spectra take place in water. Sending the radiation linearly polarized in the stent's axis direction, could increase the magnitude of the resonance. Building a smaller phantom, may reduce the signal loss.

In further experiments we are going to focus on detecting the stent fracture using MWS (already detected in open air conditions [4]) but getting closer to a human body environment.

Acknowledgments

I would like to express my special thanks of gratitude to my tutor Professor Javier Tejada, who gave me the golden opportunity to do this wonderful project on the field of medical physics, to the PhD student Gianluca Arauz-Garofalo introducing me in the world of research and helping me at every time as well as the whole group of Magnetism of *UB*.
Also be grateful to Professor Joan M.O'Callaghan of *UPC*, the doctor Oriol Rodríguez-Leor and vet Carolina Gálvez-Montón of *Hospital Germans Tries i Pujol* providing us with excellent samples.

Secondly I would also like to thank my partner, family and friends who as always helped me a lot in finishing this final degree project within the limited time.

BIBLIOGRAPHY:

[1] S. Garg and P. W. Serruys "Coronary stents: Looking forward," J. Am. Coll. Cardiol. **56**, S43-S78 (2010).

[2] J. W. Jukema *et al.*, "Restenosis after PCI. Part 1: pathohysiology and risk factors," Nat. Rev. Cardiol. **9**, 53 62 (2012).

[3] National Heart, Lung, and Blood institute "What are the Risks of Coronary Angioplasty" (http://www.nhlbi.nih.gov/)

[4] G. Arauz-Garofalo *et al*., "Microwave Spectrometry for the Evaluation of the Structural Integrity of Metallic Stents,". Med. Phys. **41**, 041902 (2014).

[5] IFAC "Dielectric properties of body tissues" (http://niremf.ifac.cnr.it/tissprop/)

[6] JXTXLX-20180, *Chengdu A-info Inc*., Chengdu, China.

[7] HP 8510C, Agilent Technologies, Santa Clara, CA, USA.

[8] Arduino Uno, *Interaction Design Institute Ivrea*, Ivrea, TO, Italy.

[9] LabVIEW 8.5, *National Instruments Corp*, Austin, TX, USA.

[10] OriginPro 8 SRO, *OriginLab Corp*., Northampton, MA, USA.

[11] Hansjörg Graf *et al.*," rf enhancement and shielding in MRI caused by conductive implants: Dependence on electrical parameters for a tube model," Med. Phys. **32**, 337-342 (2005).

[12] Hansjörg Graf *et al* "Systematics of Imaging Artifacts in MRT Caused by Metallic Vascular Implants (Stents)". Technik und Medizinphysik. **175**, 1711–1719 (2003).